

# Isoscalar giant resonances in the Sn nuclei and implications for the asymmetry term in the nuclear-matter incompressibility

T. Li, U. Garg, Y. Liu, R. Marks, B.K. Nayak, and P. V. Madhusudhana Rao  
*Physics Department, University of Notre Dame, Notre Dame, IN 46556, USA*

M. Fujiwara, H. Hashimoto, K. Nakanishi, S. Okumura, and M. Yosoi  
*Research Center for Nuclear Physics, Osaka University,  
Mihogaoka Ibaraki 10-1 Osaka, 567-0047 Japan*

M. Ichikawa, M. Itoh, R. Matsuo, and T. Terazono  
*Cyclotron and Radioisotope Center,  
Tohoku University, Sendai 980-8578, Japan*

M. Uchida  
*Tokyo Institute of Technology, 2-12-1 O-Okayama, Tokyo 152-8550, Japan*

Y. Iwao, T. Kawabata, T. Murakami, H. Sakaguchi,  
S. Terashima, Y. Yasuda, and J. Zenihiro  
*Department of Physics, Kyoto University, Kyoto 606-8502, Japan*

H. Akimune  
*Department of Physics, Konan University, Hyogo, 658-8501 Japan*

K. Kawase  
*Advanced Photon Research Center, Japan Atomic  
Energy Agency, Kizugawa, Kyoto 619-0215, Japan*

M. N. Harakeh  
*Kernfysisch Versneller Instituut, University of Groningen,  
9747 AA Groningen, The Netherlands and  
GANIL, CEA/DSM - CNRS/IN2P3, F-14076 Caen, France*

(Dated: October 25, 2018)

## Abstract

We have investigated the isoscalar giant resonances in the Sn isotopes using inelastic scattering of 386-MeV  $\alpha$ -particles at extremely forward angles, including  $0^\circ$ . We have obtained completely “background-free” inelastic-scattering spectra for the Sn isotopes over the angular range  $0^\circ$ - $9^\circ$  and up to an excitation energy of 31.5 MeV. The strength distributions for various multipoles were extracted by a multipole decomposition analysis based on the expected angular distributions of the respective multipoles. We find that the centroid energies of the isoscalar giant monopole resonance (ISGMR) in the Sn isotopes are significantly lower than the theoretical predictions. In addition, based on the ISGMR results, a value of  $K_\tau = -550 \pm 100$  MeV is obtained for the asymmetry term in the nuclear incompressibility. Constraints on interactions employed in nuclear structure calculations are discussed on the basis of the experimentally-obtained values for  $K_\infty$  and  $K_\tau$ .

## I. INTRODUCTION

Isoscalar giant resonances have been extensively studied since the discovery of the isoscalar giant quadrupole resonance (ISGQR) in the early 1970s [1–3]. The isoscalar giant monopole resonance (ISGMR) was identified in 1977 [4, 5] and was the subject of a number of studies through the 1980s [6–8]. The isoscalar giant dipole resonance (ISGDR) was first reported by Morsch et al. [9] in  $^{208}\text{Pb}$  but was conclusively identified by Davis et al. [10]. Both ISGMR and ISGDR are classified as compression modes and provide information about nuclear incompressibility,  $K_A$ , from which the incompressibility of infinite nuclear matter,  $K_\infty$ , may be obtained [11].

Most of the earlier investigations of the isoscalar giant resonances used inelastic  $\alpha$  scattering at 100–200 MeV and the strength of a particular giant resonance was assumed to be concentrated in a single peak with a Gaussian or Lorentzian shape. The resonance parameters were obtained by multiple-peak fits to the inelastic scattering spectra, after subtraction of a suitable “background” [12, 13]. In the last decade, the Texas A&M (TAMU) group has carried out  $(\alpha, \alpha')$  studies of many nuclei at a bombarding energy of 240 MeV and extracted the strength distributions of various isoscalar giant resonances in a number of nuclei [14–24] using a multipole decomposition analysis (MDA) [25]. Contemporaneously, we have carried out giant resonance measurements using inelastic scattering of 386 MeV  $\alpha$  particles at extremely small angles, including  $0^\circ$  [26–35]. An especially useful feature of our measurements has been the elimination of all instrumental background events from the inelastic scattering spectra which was rendered possible by the optical properties of the Grand Raiden spectrometer [36].

Here, we report on measurements of the isoscalar giant resonances in the even- $A$  Sn isotopes ( $A=112$ – $124$ ) over the excitation-energy range 8.5–31.5 MeV. Previously, giant resonance measurements on the Sn isotopes have been reported by the TAMU group [7, 37] and KVI group [8], using inelastic  $\alpha$  scattering at 120–130 MeV and peak-fitting analyses of spectra. More recently, the strength distributions of various isoscalar resonances have been obtained in some Sn isotopes ( $A=112, 116, 124$ ) by the TAMU group [19, 21].

High-quality measurements of the ISGMR over the full range of isotopes provide the opportunity to investigate the asymmetry term,  $K_\tau$ , of the nuclear incompressibility. This term, associated with the neutron excess ( $N - Z$ ), is crucial in obtaining the radii of neutron

stars in equation-of-state (EOS) calculations [38–41]; the asymmetry ratio,  $[(N - Z)/A]$ , changes by more than 80% over the range of the investigated Sn isotopes.

## II. EXPERIMENTAL TECHNIQUES

The experiment was performed at the ring cyclotron facility of the Research Center for Nuclear Physics (RCNP), Osaka University, using inelastic scattering of 386-MeV  $\alpha$  particles at extremely forward angles, including  $0^\circ$ . A  $^4\text{He}^{++}$  beam was accelerated by the Azimuthally Varying Field (AVF) cyclotron up to 86 MeV, injected into the  $K = 400$  ring cyclotron for acceleration up to 386 MeV, and achromatically transported to the WS experimental hall without any defining slits. To reduce the background at and near  $0^\circ$ , the beam halo has to be tuned carefully in the experiment. This was accomplished by tuning the beam profile of the injection beam for the ring cyclotron, and typically less than 1 out of 10000 events had contamination from the other bunches. The beam current was 1-20 nA, which was limited by the data acquisition rate and by the maximum available current of the accelerator. The energy resolution obtained was  $\sim 150$  keV full width at half maximum (FWHM).

Self supporting target foils of enriched even- $A$   $^{112-124}\text{Sn}$  isotopes of thickness 5.0–9.25  $\text{mg}/\text{cm}^2$  were employed; we used special target frames with a large aperture in order to reduce the background caused by the beam-halo hitting the frames. Data were also taken with a  $^{nat}\text{C}$  target at the actual field settings used in the experiments and the energy calibration was obtained from the peak positions of the 7.652- and 9.641-MeV states in the  $^{12}\text{C}(\alpha, \alpha')$  spectra.

Inelastically-scattered  $\alpha$  particles were momentum-analyzed with the high-resolution magnetic spectrometer, “Grand Raiden” [36], and the vertical and horizontal positions of the  $\alpha$  particles were measured with the focal-plane detector system comprised of two position-sensitive multi-wire drift chambers (MWDCs) and two scintillators [29]. The MWDCs and scintillators enabled us to make particle identification and to reconstruct the trajectories of the scattered particles. The scattering angle at the target and the momentum of the scattered particles were determined by the ray-tracing method. The vertical-position spectrum obtained in the double-focusing mode of the spectrometer was exploited to eliminate the instrumental background [28, 29].

Giant-resonance data were taken with the spectrometer central angle ( $\theta_{spec}$ ) set at  $0^\circ$ ,  $2.5^\circ$ ,  $3.5^\circ$ ,  $5.0^\circ$ ,  $6.5^\circ$ , and  $8.0^\circ$ , covering the angular range from  $0^\circ$  to  $9.0^\circ$  in the laboratory system. The actual angular resolution of the MWDCs, including the nominal broadening of scattering angle due to the emittance of the  $^4\text{He}^{++}$  beam and the multiple Coulomb-scattering effects, was about  $0.15^\circ$  [42]. The vertical acceptance was limited to  $\pm 20$  mr by a 2-mm-thick tantalum collimator. The energy bite of the Grand Raiden spectrometer and the special MWDC arrangements for the  $0^\circ$  measurements limited the excitation energy range observed to  $E_x=8.5\text{--}31.5$  MeV.

The incident  $^4\text{He}^{++}$  beam was stopped at three independent Faraday Cups (FC) according to the different settings of Grand Raiden [29]. In the measurements at large angles ( $\theta \geq 6.5^\circ$ ), the beam was stopped on the FC mounted inside the scattering chamber (SC-FC). For measurements at  $0^\circ$ , the FC was located downstream of the MWDCs [29]; the incident  $^4\text{He}^{++}$  particles were guided to a vacuum pipe situated at the high-momentum side of the MWDCs and finally stopped at the  $0^\circ$ -FC. A third FC was used for measurements in the scattering-angle region  $2^\circ \leq \theta \leq 5^\circ$ . This FC was installed behind the Q1-magnet of the Grand Raiden (Q1-FC) [43]. The use of these three Faraday-cups allowed us to obtain reliable values of accumulated charges for the incident  $^4\text{He}^{++}$  beam at different scattering angles. Normalization of the FCs was obtained with a beamline polarimeter located upstream from the target. The polarimeter target was inserted in the beam, and the scattered  $^4\text{He}^{++}$  particles counted, before and after each change of the FC. The overall accuracy of this normalization is estimated to be  $\sim 2\%$ , including systematic errors from slight changes in the direction of the beam during the measurement [42].

The ion-optics of the Grand Raiden spectrometer is such that the particles scattered from the target position are focused vertically and horizontally at the focal plane. Using this property, the instrumental background was completely eliminated. While inelastically scattered  $\alpha$  particles are focused at the focal plane, background events due to the rescattering of  $\alpha$  particles from the wall and pole surfaces of the spectrometer show a flat distribution in the vertical-position spectra at the focal plane, as shown in Fig. 1. The peak region in the vertical position spectrum was treated as true+background events. The off-center regions were treated as background only. Figure 2(a) shows the horizontal position spectrum for the  $^{112}\text{Sn}(\alpha, \alpha')$  reaction at  $0^\circ$ . The background spectrum has no distinct structure in the giant resonance region. Finally, we have obtained clean spectra by subtracting the background

spectrum from the true+background spectrum, as shown in Fig. 2(b).

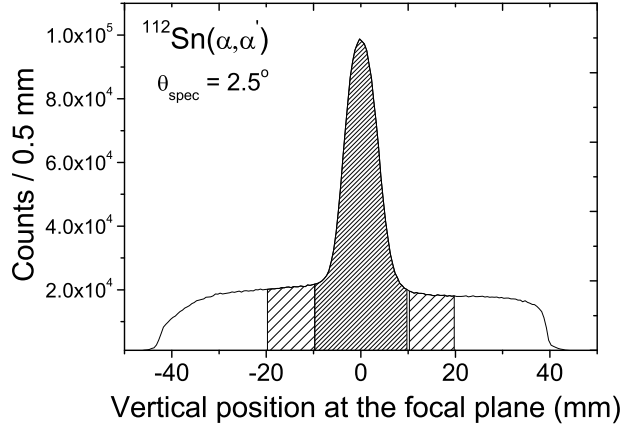


FIG. 1: Vertical-position spectrum at the focal plane of the Grand Raiden spectrometer, taken at  $2.5^\circ$ . The central densely-hatched region represents true+background events. The off-center sparsely-hatched regions represent only background events. The real events were obtained by subtracting background events from the true+background events.

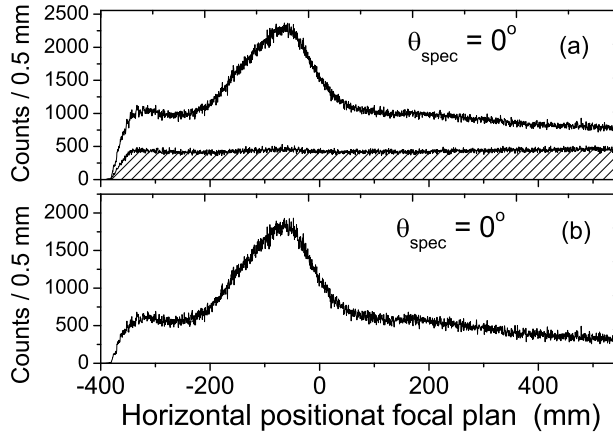


FIG. 2: (a) Horizontal-position spectrum of the  $^{112}\text{Sn}(\alpha, \alpha')$  reaction at  $0^\circ$ . The hatched region is background events. (b) Background-free spectrum

The background-free “ $0^\circ$ ” inelastic spectra for the Sn isotopes are presented in Fig. 3. In all cases, the spectrum is dominated by the ISGMR+ISGQR peak near  $E_x \sim 15$  MeV.

There is an underlying continuum in the high excitation-energy region in the spectrum; it is reasonable to assume that this continuum, remaining after elimination of the instrumental background, is primarily due to contributions from excitation of the higher multipoles and quasifree knockout processes [44].

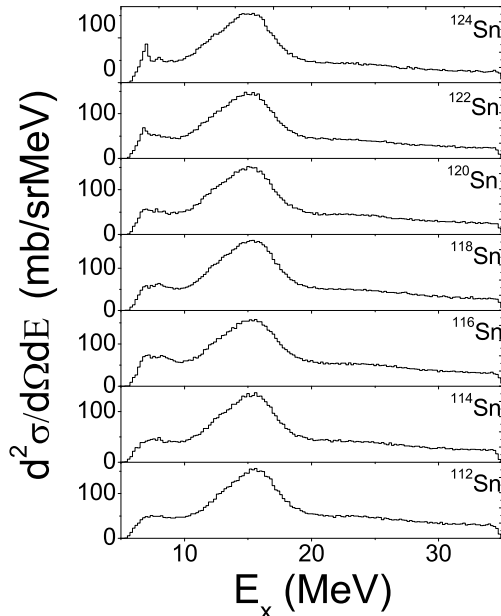


FIG. 3: Excitation-energy spectra obtained from inelastic  $\alpha$  scattering at  $\theta_{lab} = 0.69^\circ$  for all even-A Sn isotopes.

### III. DATA ANALYSIS

We have employed the MDA procedure [25] to extract the strengths of the isoscalar giant monopole resonance (ISGMR), the isoscalar giant dipole resonance (ISGDR), the isoscalar giant quadrupole resonance (ISGQR), and the high-energy octupole resonance (HEOR) in the Sn isotopes. The cross-section data were binned into 1-MeV energy intervals to reduce the statistical fluctuations. For each excitation energy bin from 8.5 MeV to 31.5 MeV, the experimental 17-point angular distribution  $\frac{d\sigma^{exp}}{d\Omega}(\theta_{cm}, E_x)$  has been fitted by means of the least-square method with the linear combination of calculated distributions  $\frac{d\sigma_L^{cal}}{d\Omega}(\theta_{cm}, E_x)$

defined by:

$$\frac{d\sigma^{exp}}{d\Omega}(\theta_{cm}, E_x) = \sum_{L=0}^7 a_L(E_x) \times \frac{d\sigma_L^{cal}}{d\Omega}(\theta_{cm}, E_x) \quad (1)$$

where  $\frac{d\sigma_L^{cal}}{d\Omega}(\theta_{cm}, E_x)$  is the calculated distorted-wave Born approximation (DWBA) cross section corresponding to 100% energy-weighted sum rule (EWSR) for the L-th multipole. The fractions of the EWSR,  $a_L(E_x)$ , for various multipole components were determined by minimizing  $\chi^2$ . This procedure is justified since the angular distributions are well characterized by the transferred angular momentum  $L$ , according to the DWBA calculations for  $\alpha$  scattering. It was confirmed that the MDA fits were not affected by including  $L > 7$ .

The DWBA calculations were performed following the method of Satchler and Khoa [45], using the density-dependent single-folding model for the real part, obtained with a Gaussian  $\alpha$ -nucleon potential, and a phenomenological Woods-Saxon potential for the imaginary term. Therefore, the  $\alpha$ -nucleus interaction is given by:

$$U(r) = V_F(r) + iW/(1 + \exp((r - R_I)/a_I)) \quad (2)$$

where  $V_F(R)$  is the real single-folding potential obtained by folding the ground-state density with the density-dependent  $\alpha$ -nucleon interaction:

$$v_{DDG}(r, r', \rho) = -v(1 - \beta\rho(r')^{2/3})\exp(-|r - r'|^2/t^2) \quad (3)$$

where  $v_{DDG}(r, r', \rho)$  is the density-dependent  $\alpha$ -nucleon interaction,  $|r - r'|$  is the distance between the center of mass of the  $\alpha$  particle and a target nucleon,  $\rho(r')$  is the ground-state density of the target nucleus at the position  $r'$  of the target nucleon,  $\beta=1.9 \text{ fm}^2$ , and  $t=1.88 \text{ fm}$ .  $W$  is the depth of the Woods-Saxon type imaginary part of the potential, with the reduced radius  $R_I$  and diffuseness  $a_I$ .

These calculations were performed with the computer code PTOLEMY [46, 47], with the input values modified [48] to take into account the correct relativistic kinematics. The shape of the real part of the potential and the form factor for PTOLEMY were obtained using the codes SDOLFIN and DOLFIN [49]. We use the transition densities and sum rules for various multipolarities described in Refs. [13, 50, 51]. The radial moments were obtained by numerical integration of the Fermi mass distribution with the parameter values from Ref. [52] (listed in Table I).



TABLE I: Fermi-distribution parameters from Ref. [52]. “c” is the adjusted half-density radius for the charge distribution and “a” is the diffuseness parameter.

Target	$^{112}\text{Sn}$	$^{114}\text{Sn}$	$^{116}\text{Sn}$	$^{118}\text{Sn}$	$^{120}\text{Sn}$	$^{122}\text{Sn}$	$^{124}\text{Sn}$
c(fm)	5.3714	5.3943	5.4173	5.4391	5.4588	5.4761	5.4907
a(fm)	0.523	0.523	0.523	0.523	0.523	0.523	0.523

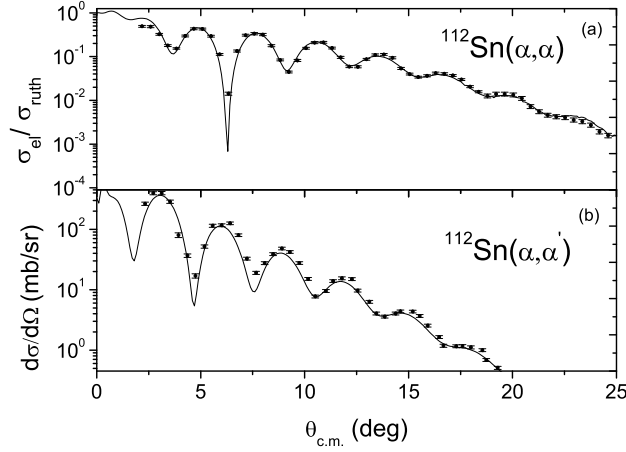


FIG. 4: (a) Ratio of the elastic  $\alpha$ -scattering cross sections to the Rutherford cross sections for  $^{112}\text{Sn}$  at 386 MeV. (b) Differential cross sections for excitation of the  $2_1^+$  state in  $^{112}\text{Sn}$ . The solid lines are the results of the folding-model calculations.

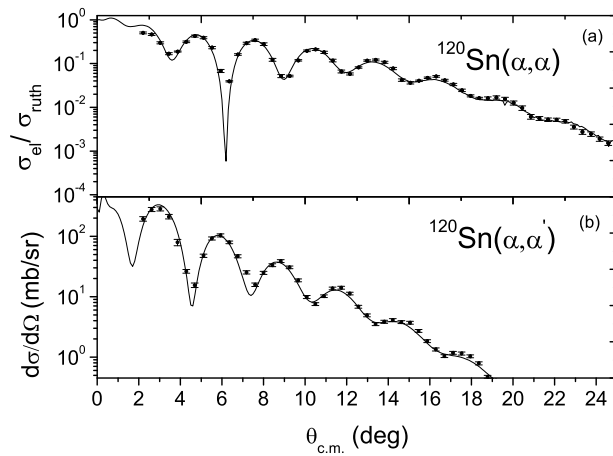


FIG. 5: Same as Fig. 4, except for  $^{120}\text{Sn}$ .

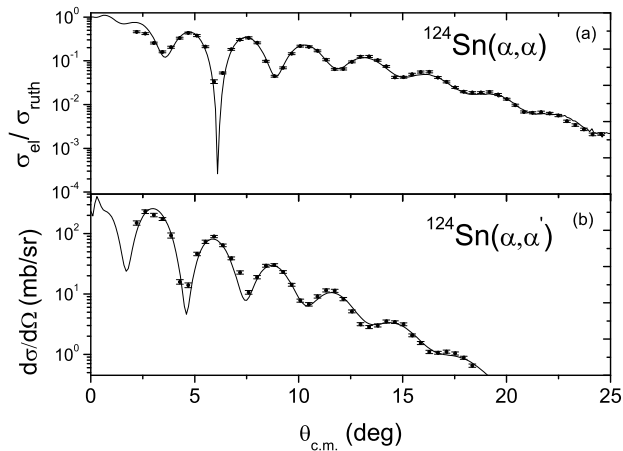


FIG. 6: Same as Fig. 4, except for  $^{124}\text{Sn}$ .

TABLE II: OM parameters obtained by fitting elastic scattering data. Also listed are the B(E2) values for the corresponding  $2_1^+$  states from Refs. [53, 54].

Target	V (MeV)	W (MeV)	$a_I$ (fm)	$R_I$ (fm)	B(E2) ( $e^2b^2$ )
$^{112}\text{Sn}$	33.9	31.7	0.60	1.02	0.24
$^{120}\text{Sn}$	33.4	33.0	0.63	1.01	0.20
$^{124}\text{Sn}$	34.0	33.5	0.61	1.02	0.17

The optical-model (OM) parameters *viz.* the real part of the potential ( $V_F(r)$ ), the Woods-Saxon type imaginary part of potential ( $W$ ), the reduced radius ( $R_I$ ), and the diffuseness ( $a_I$ ) in Eq. 2 were determined by fitting the differential cross sections of elastic  $\alpha$  scattering measured for  $^{112}\text{Sn}$ ,  $^{120}\text{Sn}$ , and  $^{124}\text{Sn}$  in a companion experiment; the results are listed in Table II. The OM fits to the elastic scattering data for  $^{112}\text{Sn}$ ,  $^{120}\text{Sn}$ , and  $^{124}\text{Sn}$ , are shown in Figs. 4(a), 5(a), and 6(a), respectively. To test the efficacy of the OM parameters, DWBA calculations were carried out for the first  $2^+$  states in these nuclei using a collective form factor and previously-established B(E2) values obtained from Refs. [53, 54] (also listed in Table II). Figures. 4(b), 5(b), and 6(b) compare the results of these calculations with the experimental data; indeed, the DWBA calculations reproduce the experimental differential cross sections for the  $2_1^+$  states well without any normalization.

The contribution of the IVGDR excitation to the measured cross sections was subtracted

prior to multipole decomposition. Cross sections for exciting the IVGDR were obtained with DWBA calculations on the basis of the Goldhaber-Teller model and using the strength distribution obtained from photonuclear work [55].

Figs. 7 and 8 show the MDA fits to the experimental angular distributions of the differential cross sections for the 16.5-MeV and 25.5-MeV energy bins in the inelastic-scattering spectra of  $^{112}\text{Sn}$  and  $^{124}\text{Sn}$ , respectively, along with the contributions from the  $L=0, 1$  and  $2$  multipoles. The ISGMR contribution is dominant in comparison to the other multipoles at  $E_x=16.5$  MeV. On the other hand, the ISGDR is the dominant contributor at  $E_x=25.5$  MeV.

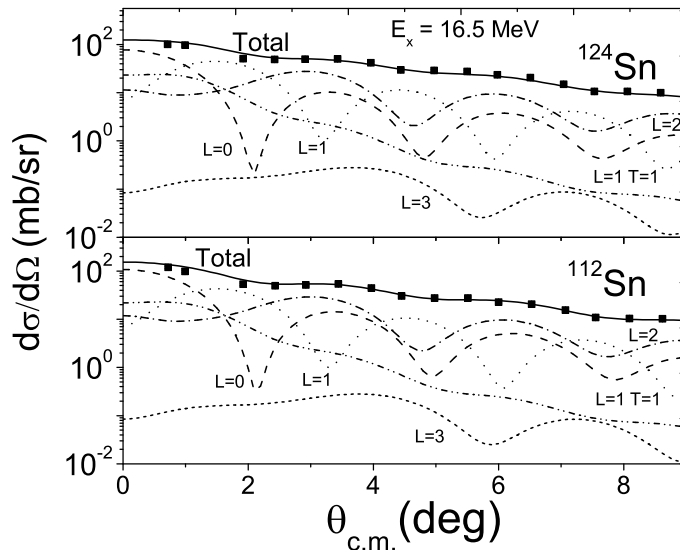


FIG. 7: Angular distribution of 1-MeV bins centered at  $E_x=16.5$  MeV for  $^{112}\text{Sn}(\alpha,\alpha')$  and  $^{124}\text{Sn}(\alpha,\alpha')$ . The solid squares are the experimental data and the solid lines are the MDA fits to the data. Also shown are the contributions to the fits from  $L=0$  (dashed line),  $L=1$  (dotted line),  $L=2$  (dash-dotted line) and  $L=3$  (small-dashed line) multipoles, as well as from the IVGDR (dash-dot-dotted line).

#### IV. RESULTS AND DISCUSSION

We have extracted strength distributions for  $L=0, 1, 2,$  and  $3$  multipoles over the energy range 8.5 MeV–31.5 MeV in all the Sn isotopes investigated in this work. These are displayed

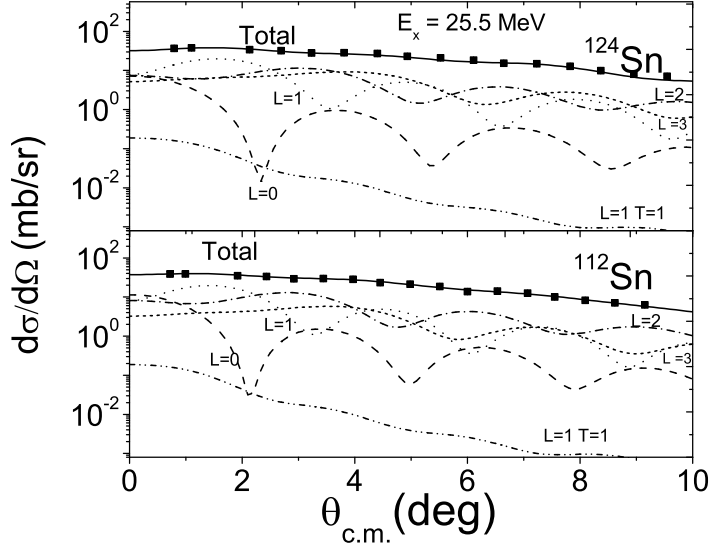


FIG. 8: Same as Fig. 7 except for the 25.5-MeV energy bin (see text).

in Figs. 9, 10, 11, and 12, respectively. The strengths are related to the coefficients  $a_L$  in Eq. 1 as (see, Refs. [13, 51]):

$$S_0(E_x) = \frac{2\hbar^2 A \langle r^2 \rangle}{mE_x} a_0(E_x) \quad (4)$$

$$S_1(E_x) = \frac{3\hbar^2 A}{32\pi m E_x} \left( 11 \langle r^4 \rangle - \frac{25}{3} \langle r^2 \rangle^2 - 10\epsilon \langle r^2 \rangle \right) a_1(E_x) \quad (5)$$

$$S_{L \geq 2}(E_x) = \frac{\hbar^2 A}{8\pi m E_x} L(2L+1)^2 \langle r^{2L-2} \rangle a_2(E_x) \quad (6)$$

where  $m$ ,  $A$  and  $\langle r^N \rangle$  are the nucleon mass, the mass number, and the  $N$ th moment of the ground-state density, and  $\epsilon = (4/E_2 + 5/E_0)\hbar^2/3mA$ ;  $E_0$  and  $E_2$  are the centroid energies of the ISGMR and the ISGQR and have been taken as  $80 A^{-1/3}$  MeV and  $64 A^{-1/3}$  MeV, respectively.

It should be noted that although we employed calculated DWBA cross sections with up to  $L=7$  in the MDA fitting procedure, it was not possible to reliably extract the strength distributions for  $L \geq 4$  because of the limited angular range ( $0^\circ$ – $9^\circ$ ). Further, there is a small, near-constant ISGMR and ISGQR strength up to the highest excitation energies measured

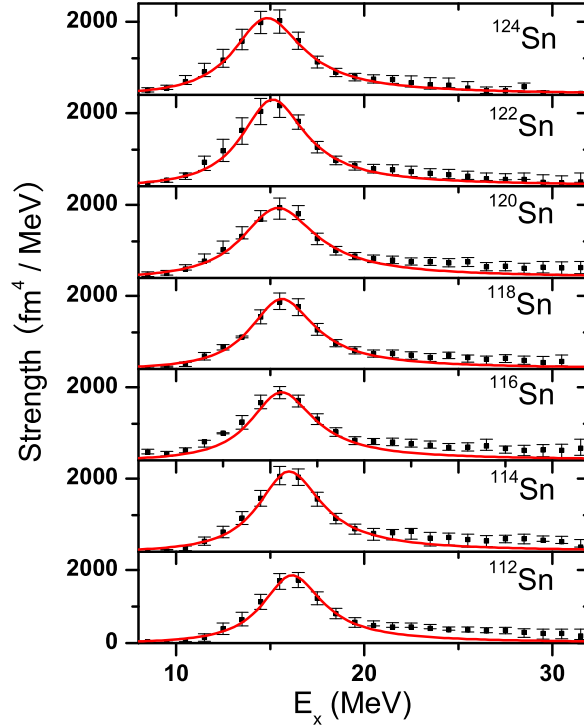


FIG. 9: (Color online) ISGMR strength distributions obtained for the Sn isotopes in the present experiment. Error bars represent the uncertainties from fitting the angular distributions in the MDA procedure. The solid lines show Lorentzian fits to the data.

in this experiment. The *raison d'être* of this extra strength is not quite well understood. However, similarly enhanced E1 strengths at high excitation energies were noted previously [29, 30] and have been attributed to contributions to the continuum from three-body channels, such as knockout reactions [44]. These processes are implicitly included in the MDA as background and may lead to spurious contributions to the extracted multipole strengths at higher energies where the associated cross sections are very small. This conjecture is supported by measurements of proton decay from the ISGDR at backward angles wherein no such spurious strength is observed in spectra in coincidence with the decay protons [31, 56–58]; quasifree knockout results in protons that are forward peaked. A similar increase in the ISGMR strength at high excitation energies was reported as well by the TAMU group in  $^{12}\text{C}$  when they carried out MDA without subtracting the continuum from the excitation-energy spectra [18].

The  $L = 0$  strength distributions were fitted with a Lorentzian function to determine the centroid energies and widths of the ISGMR. These fits are shown superimposed in

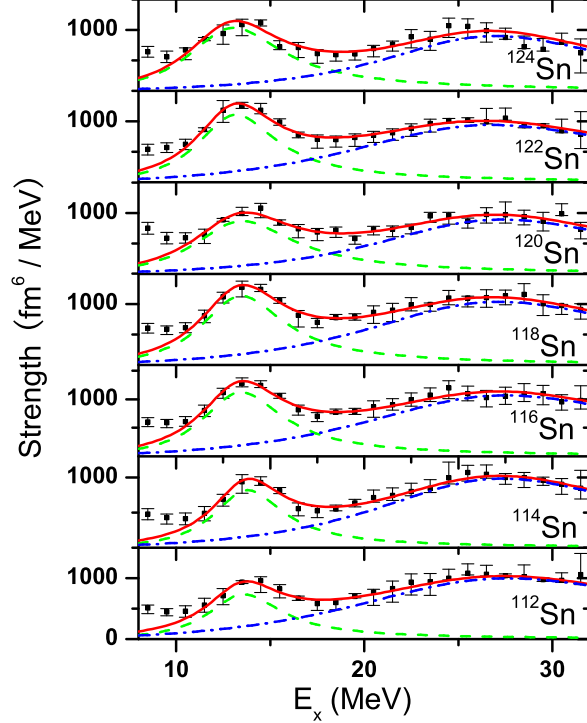


FIG. 10: (Color online) ISGDR strength distributions obtained for the Sn isotopes in the present experiment. Error bars represent the uncertainties from fitting the angular distributions in the MDA procedure. The solid lines show Lorentzian fits to the data.

Fig. 9; the corresponding fitting parameters are presented in Table III and compared with results from TAMU [19, 21]. In this and subsequent comparisons and discussion, we refer only to the recent TAMU results because those are from comparable data and analysis—all other previous results on the Sn isotopes were from peak-fitting analyses of data taken at significantly lower energies.

In order to compare with the available theoretical results, various moment ratios for the experimental ISGMR strength distributions have been calculated over the excitation-energy range,  $E_x = 10.5\text{--}20.5$  MeV, encompassing the ISGMR peak. The results are listed in Table IV. The reasons for the difference between the present results and those from TAMU for  $^{112}\text{Sn}$  and  $^{124}\text{Sn}$  are not readily apparent but might be attributable to the fact that in their analysis the multipole decomposition is carried out after subtracting a “background” from the excitation-energy spectrum, whereas, as pointed out earlier, no such subtraction is required in the present analysis since the  $\text{Sn}(\alpha, \alpha')$  spectra obtained in our work have been rendered free of all instrumental background events.

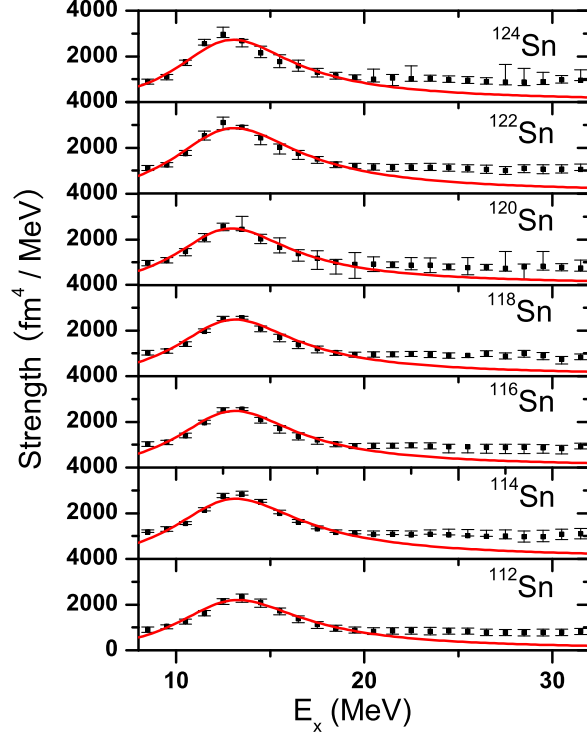


FIG. 11: (Color online) ISGQR strength distributions obtained for the Sn isotopes in the present experiment. Error bars represent the uncertainties from fitting the angular distributions in the MDA procedure. The solid lines show Lorentzian fits to the data.

Figure 10 shows the strength distributions of ISGDR. We observe a “bi-modal” distribution between  $E_x=8.5$  MeV and  $E_x=31.5$  MeV. This bi-modal pattern for the ISGDR has been observed in all nuclei investigated so far, both in the RCNP and TAMU measurements. This “low-energy” isoscalar  $L=1$  strength (LE) has engendered considerable interest and argument over the past few years. It is present in nearly all of the recent theoretical calculations in some form or the other, and at similar energies, although with varying strength. It has been shown [59, 60] that the centroid of this component of the  $L=1$  strength is independent of the nuclear incompressibility and while the exact nature of this component is not fully understood yet, suggestions have been extended to the effect that this component might represent the “toroidal” [60, 61] or the “vortex” modes [62]. It is impossible to distinguish between the competing possibilities based on currently-available data [31]. There is general agreement, however, that only the high-energy (HE) component of this bi-modal distribution needs to be considered in obtaining a value of  $K_\infty$  from the energy of the ISGDR. The strength distributions of the ISGDR, therefore, have been fitted

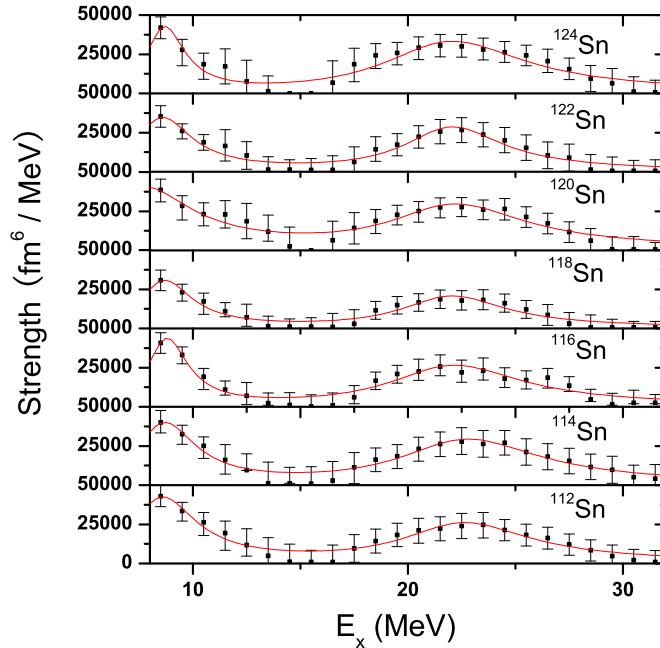


FIG. 12: (Color online) HEOR strength distributions obtained for the Sn isotopes in the present experiment. Error bars represent the uncertainties from fitting the angular distributions in the MDA procedure. The solid lines show Lorentzian fits to the data.

with a two-Lorentzian function and the fitting parameters for the LE- and HE-components are presented in Tables V and VI, respectively. It may be noted that because of the “spurious” strength at the higher excitation energies mentioned previously, the numbers for the extracted EWSR are significantly larger than 100% in some cases.

The strength distributions of the ISGQR are shown in Fig. 11. These too were fitted with a Lorentzian function to determine the centroid energies and the widths. The fit parameters are presented in Table VII.

The  $L=3$  strength distributions (Fig. 12) show an enhanced strength at  $E_x < 10$  MeV. This part is, most likely, from the low-energy octupole resonance (LEOR). The LEOR represents the  $1\hbar\omega$  component of the  $L=3$  strength and has been reported in a number of nuclei previously [63, 64]. The strength distributions were, therefore, fitted with a two-Lorentzian function to determine the centroid energy of HEOR (the high-excitation-energy component). The extracted HEOR peak-energies are presented in Table VIII.



TABLE III: Lorentzian-fit parameters for the ISGMR strength distributions in the Sn isotopes, as extracted from MDA. The quoted EWSR values are from the fitted Lorentzians. The results from TAMU work (from Gaussian fits), where available, are provided for comparison [19, 21].

Target	$E_{ISGMR}$ (MeV)	$\Gamma$ (MeV)	EWSR <sup>a</sup>	Reference
<sup>112</sup> Sn	$16.1 \pm 0.1$	$4.0 \pm 0.4$	$0.92 \pm 0.04$	This work
	$15.67^{+0.11}_{-0.11}$	$5.18^{+0.40}_{-0.04}$	$1.10^{+0.15}_{-0.12}$	TAMU
<sup>114</sup> Sn	$15.9 \pm 0.1$	$4.1 \pm 0.4$	$1.04 \pm 0.06$	This work
<sup>116</sup> Sn	$15.8 \pm 0.1$	$4.1 \pm 0.3$	$0.99 \pm 0.05$	This work
<sup>118</sup> Sn	$15.6 \pm 0.1$	$4.3 \pm 0.4$	$0.95 \pm 0.05$	This work
<sup>120</sup> Sn	$15.4 \pm 0.2$	$4.9 \pm 0.5$	$1.08 \pm 0.07$	This work
<sup>122</sup> Sn	$15.0 \pm 0.2$	$4.4 \pm 0.4$	$1.06 \pm 0.05$	This work
<sup>124</sup> Sn	$14.8 \pm 0.2$	$4.5 \pm 0.5$	$1.05 \pm 0.06$	This work
	$15.34^{+0.13}_{-0.13}$	$5.00^{+0.13}_{-0.53}$	$1.06^{+0.10}_{-0.20}$	TAMU

<sup>a</sup>Only statistical uncertainties are included; systematic errors, mostly from DWBA calculations, are  $\sim 15\%$ .

The primary focus of this work has been on the ISGMR because of its direct connection with the nuclear incompressibility. The excitation energy of the ISGMR is expressed in the scaling model [70] as:

$$E_{ISGMR} = \hbar \sqrt{\frac{K_A}{m \langle r^2 \rangle}} \quad (7)$$

where  $m$  is the nucleon mass,  $\langle r^2 \rangle$  the ground-state mean-square radius, and  $K_A$ , the incompressibility of the nucleus.

The moment ratios,  $m_1/m_0$ , for the ISGMR strengths in the Sn isotopes are shown in Fig. 13 and compared with recent theoretical results from Colò *et al.* (non-relativistic) [65, 66] and Piekarewicz (relativistic) [67]. The calculations overestimate the experimental ISGMR energies significantly (by almost 1 MeV in case of the higher-A isotopes!). This difference is very surprising since the interactions used in these calculations are those that very closely reproduce the ISGMR energies in <sup>208</sup>Pb and <sup>90</sup>Zr. Indeed, this disagreement leaves open a puzzling question: Why are the tin isotopes so soft [67]? Are there any nuclear structure effects that need to be taken into account to describe the ISGMR energies in the Sn isotopes? Or, more provocatively, do the ISGMR energies depend on something more

TABLE IV: Various moment ratios for the ISGMR strength distributions in the Sn isotopes. All moments have been calculated over  $E_x = 10.5\text{--}20.5$  MeV. The quoted EWSR values are from the strength observed within this energy range. The results from TAMU work, where available, are provided for comparison [19, 21].

Target	$\frac{m_1}{m_0}$ (MeV)	$\sqrt{\frac{m_3}{m_1}}$ (MeV)	$\sqrt{\frac{m_1}{m_{-1}}}$ (MeV)	EWSR <sup>a</sup>	Reference
<sup>112</sup> Sn	$16.2 \pm 0.1$	$16.7 \pm 0.2$	$16.1 \pm 0.1$	$0.73 \pm 0.04$	This work
	$15.43^{+0.11}_{-0.10}$	$16.05^{+0.26}_{-0.14}$	$15.23^{+0.10}_{-0.10}$	$1.16^{+0.13}_{-0.18}$	TAMU
<sup>114</sup> Sn	$16.1 \pm 0.1$	$16.5 \pm 0.2$	$15.9 \pm 0.1$	$0.86 \pm 0.05$	This work
<sup>116</sup> Sn	$15.8 \pm 0.1$	$16.3 \pm 0.2$	$15.7 \pm 0.1$	$0.86 \pm 0.05$	This work
	$15.85 \pm 0.20$			$1.12 \pm 0.15$	TAMU
<sup>118</sup> Sn	$15.8 \pm 0.1$	$16.3 \pm 0.1$	$15.6 \pm 0.1$	$0.73 \pm 0.04$	This work
<sup>120</sup> Sn	$15.7 \pm 0.1$	$16.2 \pm 0.2$	$15.5 \pm 0.1$	$0.78 \pm 0.05$	This work
<sup>122</sup> Sn	$15.4 \pm 0.1$	$15.9 \pm 0.2$	$15.2 \pm 0.1$	$0.85 \pm 0.05$	This work
<sup>124</sup> Sn	$15.3 \pm 0.1$	$15.8 \pm 0.1$	$15.1 \pm 0.1$	$0.77 \pm 0.05$	This work
	$14.50^{+0.14}_{-0.14}$	$14.96^{+0.10}_{-0.11}$	$14.33^{+0.17}_{-0.14}$	$1.04^{+0.11}_{-0.11}$	TAMU

<sup>a</sup>Only statistical uncertainties are included; systematic errors, mostly from DWBA calculations, are  $\sim 15\%$ .

than the nuclear incompressibility, requiring a modification of the scaling relationship given in Eq. 7?

There have been several attempts to explain this anomaly. One of the earliest was by Civitarese *et al.* [71] to estimate the effect of pairing correlations on the energy of the ISGMR. The shifts obtained for the ISGMR energies of 100–150 keV across the Sn isotopic chain were insufficient to explain the experimental data. Piekarewicz and Centelles [72] have constructed a hybrid model having the same incompressibility coefficient ( $K_\infty=230$  MeV) as the FSUGold [73] while preserving the stiff symmetry energy of NL3 [74]. This results in a considerably softer incompressibility coefficient for neutron-rich matter and produces a significant improvement in agreement with the experimental data on the ISGMR's in the Sn isotopes. However, as the authors point out, while the improvement in case of the Sn isotopes is unquestionable, an important problem remains: the hybrid model underestimates the ISGMR centroid energy in <sup>208</sup>Pb by almost 1 MeV, suggesting that the rapid softening

TABLE V: Lorentzian-fit parameters for the low-energy component of ISGDR strength distributions in the Sn isotopes, as extracted from MDA. The results from TAMU work, where available, are provided for comparison [19, 21].

Target	$E_{LE-ISGDR}$ (MeV)	$\Gamma$ (MeV)	Reference
$^{112}\text{Sn}$	$15.4 \pm 0.1$	$4.9 \pm 0.5$	This work
	$14.92^{+0.15}_{-0.14}$	$8.82^{+0.26}_{-0.29}$	TAMU
$^{114}\text{Sn}$	$15.0 \pm 0.1$	$5.6 \pm 0.5$	This work
$^{116}\text{Sn}$	$14.9 \pm 0.1$	$5.9 \pm 0.5$	This work
	$14.38 \pm 0.25$	$5.84 \pm 0.30$	TAMU
$^{118}\text{Sn}$	$14.8 \pm 0.1$	$6.1 \pm 0.3$	This work
$^{120}\text{Sn}$	$14.7 \pm 0.1$	$5.9 \pm 0.3$	This work
$^{122}\text{Sn}$	$14.4 \pm 0.1$	$6.7 \pm 0.3$	This work
$^{124}\text{Sn}$	$14.3 \pm 0.1$	$6.6 \pm 0.3$	This work
	$13.31^{+0.15}_{-0.15}$	$6.60^{+0.15}_{-0.13}$	TAMU

with neutron excess predicted by this hybrid model might be unrealistic. They also suggest that the failure of the FSUGold to reproduce the ISGMR energies might be due to missing physics unrelated to the incompressibility of neutron-rich nuclear matter; as an example of such missing physics, they mention the superfluid character of the Sn isotopes resulting from their open-shell structure.

Calculations have also become available recently from the RMF approach with the DD-ME2 interaction [75], and these reproduce the centroids of the ISGMR in the Sn isotopes rather well [68]. It is also seen that the DD-ME2 interaction falls within the constraints imposed by the experimental  $K_\infty$  and  $K_\tau$  values (see discussion below). Some concern has been expressed, however, that this agreement of the centroid energies might be just a coincidence since the ISGMR strength distributions for the Sn isotopes from this work appear to be not significantly different from those obtained from, for example, the FSUGold [76].

In calculations using the T5 Skyrme interaction within the quasiparticle time blocking approximation (QTBA) approach, Tselyaev *et al.* [69] have obtained the ISGMR strength distributions in all the Sn isotopes in good agreement with the experimental data, including the resonance widths. However, T5 has the associated  $K_\infty$  value of only 202 MeV, which is

TABLE VI: Lorentzian-fit parameters for the high-energy component of ISGDR strength distributions in the Sn isotopes, as extracted from MDA. The results from TAMU work, where available, are provided for comparison [19, 21].

Target	$E_{HE-ISGDR}$ (MeV)	$\Gamma$ (MeV)	EWSR <sup>a</sup>	Reference
<sup>112</sup> Sn	$26.2 \pm 0.8$	$16.3 \pm 4.0$	$1.02 \pm 0.03$	This work
	$26.28^{+0.32}_{-0.23}$	$10.82^{+0.39}_{-0.36}$	$0.70^{+0.10}_{-0.10}$	TAMU
<sup>114</sup> Sn	$26.1 \pm 0.8$	$13.9 \pm 3.4$	$1.23 \pm 0.03$	This work
<sup>116</sup> Sn	$25.9 \pm 0.6$	$13.1 \pm 4.2$	$1.02 \pm 0.03$	This work
	$25.50 \pm 0.60$	$12.00 \pm 0.60$	$0.88 \pm 0.20$	TAMU
<sup>118</sup> Sn	$26.0 \pm 0.3$	$13.1 \pm 2.0$	$1.20 \pm 0.03$	This work
<sup>120</sup> Sn	$26.0 \pm 0.4$	$13.1 \pm 1.9$	$1.50 \pm 0.03$	This work
<sup>122</sup> Sn	$26.3 \pm 0.2$	$12.4 \pm 1.1$	$1.47 \pm 0.03$	This work
<sup>124</sup> Sn	$25.7 \pm 0.5$	$10.2 \pm 1.6$	$1.29 \pm 0.06$	This work
	$25.06^{+0.22}_{-0.21}$	$13.87^{+0.28}_{-0.22}$	$0.93^{+0.12}_{-0.13}$	TAMU

<sup>a</sup>Only statistical uncertainties are included; systematic errors, mostly from DWBA calculations and the contributions at the highest energies (see text), are  $\sim 30\%$ .

significantly lower than that extracted earlier from the ISGMR’s in <sup>208</sup>Pb and <sup>90</sup>Zr. While the agreement with the experimental data is impressive (and, indeed, reproduces the A-dependence rather well), it does leave the question of “softness” of the Sn nuclei unanswered. As the authors themselves state, the goal of their work has not been to solve the problem of the nuclear-matter incompressibility but to find under which conditions one can obtain reasonable description of the experimental data for the considered tin isotopes.

The “superfluid” character of the Sn isotopes, resulting from pairing correlations in open-shell nuclei, has been investigated by Li *et al.* [77]. In a self-consistent QRPA model that employs the canonical HFB basis and an energy-density functional with a Skyrme mean-field part and density-dependent pairing, they calculated the energy of the ISGMR for the Sn isotopes and looked at the effects of different kinds of pairing forces (volume, surface, and mixed). They find that, compared with the HF+RPA and HF-BCS-QRPA formalisms, the HFB+QRPA calculations lead to energies for the ISGMR in Sn isotopes

TABLE VII: Lorentzian-fit parameters of ISGQR strength distributions in the Sn isotopes, as extracted from MDA. The results from TAMU work, where available, are provided for comparison [19, 21].

Target	$E_{ISGQR}$ (MeV)	$\Gamma$ (MeV)	EWSR <sup>a</sup>	Reference
<sup>112</sup> Sn	$13.4 \pm 0.1$	$7.0 \pm 0.5$	$1.08 \pm 0.04$	This work
	$13.48^{+0.15}_{-0.14}$	$4.90^{+0.22}_{-0.27}$	$0.88^{+0.14}_{-0.13}$	TAMU
<sup>114</sup> Sn	$13.2 \pm 0.1$	$6.8 \pm 0.4$	$1.25 \pm 0.05$	This work
<sup>116</sup> Sn	$13.1 \pm 0.1$	$6.4 \pm 0.4$	$1.12 \pm 0.04$	This work
	$13.50 \pm 0.35$	$5.00 \pm 0.30$	$1.08 \pm 0.12$	TAMU
<sup>118</sup> Sn	$13.1 \pm 0.1$	$6.6 \pm 0.3$	$1.08 \pm 0.03$	This work
<sup>120</sup> Sn	$12.9 \pm 0.1$	$7.0 \pm 0.7$	$1.04 \pm 0.04$	This work
<sup>122</sup> Sn	$12.8 \pm 0.1$	$7.8 \pm 0.6$	$1.25 \pm 0.04$	This work
<sup>124</sup> Sn	$12.6 \pm 0.1$	$7.7 \pm 0.9$	$1.13 \pm 0.04$	This work
	$12.72^{+0.11}_{-0.11}$	$4.20^{+0.32}_{-0.03}$	$0.89^{+0.15}_{-0.10}$	TAMU

<sup>a</sup>Only statistical uncertainties are included; systematic errors, mostly from DWBA calculations, are  $\sim 20\%$ .

that are significantly closer to the experimental values, in particular with the surface pairing forces and the SKM\* interaction ( $K_\infty \sim 215$  MeV) [78]. Thus, while pairing effects lower the ISGMR excitation energies, one still needs to reduce the  $K_\infty$  value by  $\sim 10\%$  for achieving a reasonable agreement with the experimental data.

A very intriguing possibility in explaining the “softness” of the Sn isotopes has been offered very recently by Khan [79, 80]. The author asserts that, in analogy with the mutually-enhanced-magicity (MEM) effect observed in predictions of masses with different energy-density functionals [81, 82], the ISGMR energy in the doubly-magic nuclei might be anomalously higher. The obvious implication is that the calculations using interactions that are successful in describing the ISGMR in the doubly-magic nucleus <sup>208</sup>Pb would necessarily overestimate the ISGMR energies in the open-shell nuclei. If this effect is manifested in any significant way, the energy of the ISGMR in the non-doubly-magic Pb isotopes, <sup>204</sup>Pb and <sup>206</sup>Pb, would be measurably lower than that in <sup>208</sup>Pb [80]. In the only measurement of the ISGMR in <sup>206</sup>Pb reported so far [83], this conjecture does not appear to hold. Still, precise

TABLE VIII: Lorentzian-fit parameters of HEOR strength distributions in the Sn isotopes, as extracted from MDA. The results from TAMU work, where available, are provided for comparison [19, 21].

Target	$E_{HEOR}$ (MeV)	$\Gamma$ (MeV)	Reference
$^{112}\text{Sn}$	$22.7 \pm 0.7$	$7.2 \pm 1.9$	This work
	$20.63^{+0.30}_{-0.28}$	$3.21^{+0.30}_{-0.28}$	TAMU <sup>a</sup>
$^{114}\text{Sn}$	$22.7 \pm 0.7$	$7.2 \pm 2.1$	This work
$^{116}\text{Sn}$	$22.3 \pm 0.6$	$7.6 \pm 1.7$	This work
	$23.3 \pm 0.8$	$10.9 \pm 0.6$	TAMU
$^{118}\text{Sn}$	$22.1 \pm 0.6$	$5.9 \pm 1.5$	This work
$^{120}\text{Sn}$	$22.3 \pm 0.6$	$7.5 \pm 1.8$	This work
$^{122}\text{Sn}$	$22.1 \pm 0.6$	$5.6 \pm 1.5$	This work
$^{124}\text{Sn}$	$22.1 \pm 0.5$	$8.1 \pm 1.5$	This work
	$19.12^{+0.26}_{-0.26}$	$3.30^{+0.17}_{-0.05}$	TAMU <sup>a</sup>

<sup>a</sup>( $m_1/m_0$ ) ratios.

measurements of the ISGMR in the Pb isotopes, using background-free inelastic spectra with high-energy  $\alpha$  beams, would be worthwhile to fully examine this possibility.

The incompressibility of a nucleus,  $K_A$ , may be expressed as:

$$K_A \sim K_{vol}(1 + cA^{-1/3}) + K_\tau((N - Z)/A)^2 + K_{Coul}Z^2A^{-4/3} \quad (8)$$

Here,  $c \approx -1$ [84], and  $K_{Coul}$  is essentially model independent (in the sense that the deviations from one theoretical model to another are quite small), so that the associated term can be calculated for a given isotope. Thus, for a series of isotopes, the difference  $K_A - K_{Coul}Z^2A^{-4/3}$  may be approximated to have a quadratic relationship with the asymmetry parameter, of the type  $y = A + Bx^2$ , with  $K_\tau$  being the coefficient, B, of the quadratic term. It has been established previously [85, 86] that direct fits to the Eq. 8 do not provide good constraints on the value of  $K_\infty$ . However, this expression is being used here not to obtain a value for  $K_\infty$ , but, rather, only to demonstrate the approximately quadratic relationship between  $K_A$  and the asymmetry parameter.

From such an analysis of the ISGMR data in the Sn isotopes, we have obtained a value of

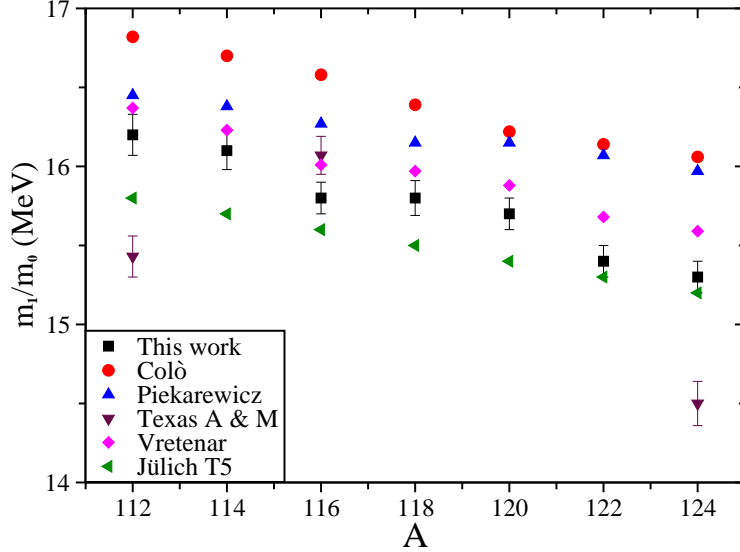


FIG. 13: (Color online) Systematics of the moment ratios  $m_1/m_0$  for the ISGMR strength distributions in the Sn isotopes. The experimental results (filled squares) are compared with results from non-relativistic RPA calculations (without pairing) by Colò *et al.* [65, 66] (filled circles); relativistic calculations of Piekarewicz [67] (triangles); RMF calculations from Vretenar *et al.* [68] (diamonds); and, QTBA calculations from the Jülich group [69] (sideways triangles). Results for  $^{112}\text{Sn}$ ,  $^{116}\text{Sn}$  and  $^{124}\text{Sn}$  reported by the TAMU group [19, 21] are also shown (inverted triangles).

$K_\tau = -550 \pm 100$  MeV (see Fig. 4 in Ref. [34]). This number is consistent with the value of  $K_\tau = -370 \pm 120$  MeV obtained from an analysis of the isotopic transport ratios in medium-energy heavy-ion reactions [87]. Incidentally, this value has been modified from the value of  $-500 \pm 50$  MeV that was quoted previously by this group [88, 89] and referred to in Ref. [34]. It transpires that they had identified the quantity that they had obtained,  $K_{asy}$ , as being identical to  $K_\tau$ , the quantity that has been obtained from the ISGMR measurements; the two differ by a higher-order term [87, 90]. More recently, a value of  $K_\tau = -500^{+125}_{-100}$  MeV has been obtained by Centelles *et al.* [91] from constraints put by neutron-skin data from anti-protonic atoms across the mass table; here again, it would appear that what the authors have termed  $K_\tau$  is actually the aforementioned  $K_{asy}$ . Further, a value of  $K_\tau = -500 \pm 50$  MeV has been obtained also by Sagawa *et al.* by comparing our Sn ISGMR data with calculations using different Skyrme Hamiltonians and RMF Lagrangians [92]. The  $K_\tau$  value obtained from our ISGMR measurements has, thus, been verified by a number of different procedures involving quite different data. A more precise determination of  $K_\tau$  will likely result from extending

the ISGMR measurements to longer isotopic chains. This provides strong motivation for measuring the ISGMR strength in unstable nuclei, a focus of current investigations at the new rare isotope beam facilities at RIKEN, GANIL, GSI, and NSCL [93–96].

Combined with the value of  $K_\infty = 240 \pm 10$  MeV obtained from the ISGMR and ISGDR data [31, 65, 73, 97], we now have “experimental” values of both  $K_\infty$  and  $K_\tau$  which, together, can provide a means of selecting the most appropriate of the interactions used in EOS calculations. For example, this combination of “experimental” values for  $K_\infty$  and  $K_\tau$  essentially rules out a vast majority of the Skyrme-type interactions currently in use in nuclear structure calculations [90, 98]. Similar conclusions were reached for EOS equations in Refs. [99, 100].

## V. SUMMARY

We have measured the strength distributions of the isoscalar giant resonances (ISGMR, ISGDR, ISGQR, and HEOR) in the even-A  $^{112-124}\text{Sn}$  isotopes via inelastic scattering of 386-MeV  $\alpha$  particles at extremely forward angles, including  $0^\circ$ . The extracted parameters for these resonances are in good agreement with previously-obtained values where available. The ISGMR centroid energies are significantly lower than those predicted for these isotopes by recent calculations and point to the need for further theoretical exploration of applicable nuclear structure effects, especially the role of pairing in ISGMR strength calculations in the open-shell nuclei. The asymmetry-term,  $K_\tau$ , in the expression for the nuclear incompressibility has been determined to be  $-550 \pm 100$  MeV from the ISGMR data in Sn isotopes and is found to be consistent with a number of indirectly extracted values for this parameter.

## VI. ACKNOWLEDGMENTS

We wish to thank the RCNP staff for providing high-quality  $\alpha$  beams required for these measurements. This work has been supported in part by the US-Japan Cooperative Science Program of the JSPS, and by the National Science Foundation (Grants No. INT03-42942,



- [1] R. Pitthan and T. Walcher, Phys. Lett. **36B**, 563 (1971).
- [2] S. Fukuda and Y. Torizuka, Phys. Rev. Lett. **29**, 1109 (1972).
- [3] M. B. Lewis and F. E. Bertrand, Nucl. Phys. A **196**, 337 (1972).
- [4] M. N. Harakeh *et al.*, Phys. Rev. Lett. **38**, 686 (1977).
- [5] D. H. Youngblood *et al.*, Phys. Rev. Lett. **39**, 1188 (1977).
- [6] A. van der Woude, Int. Rev. Nucl. Phys. **7**, 100 (1991).
- [7] D. H. Youngblood, P. Bogucki, J. D. Bronson, U. Garg, Y.-W. Lui, and C. M. Rozsa, Phys. Rev. C **23**, 1997 (1981).
- [8] M. M. Sharma *et al.*, Phys. Rev. C **38**, 2562 (1988).
- [9] H. P. Morsch, M. Rogge, P. Turek, and C. Mayer-Borricke, Phys. Rev. Lett. **45**, 337 (1980).
- [10] B. F. Davis *et al.*, Phys. Rev. Lett. **79**, 607 (1997).
- [11] J. Blaizot *et al.*, Nucl. Phys. A **591**, 435 (1995).
- [12] J. Speth, *Electric and Magnetic Giant Resonances in Nuclei* (World Scientific, Singapore, 1991).
- [13] M. N. Harakeh and A. van der Woude, *Giant Resonances: Fundamental High-Frequency Modes of Nuclear Excitation* (Oxford Univ. Press, New York, 2001).
- [14] D. H. Youngblood *et al.*, Phys. Rev. Lett. **82**, 691 (1999).
- [15] D. H. Youngblood *et al.*, Phys. Rev. C **60**, 014304 (1999).
- [16] H. L. Clark, Y.-W. Lui, and D. H. Youngblood, Phys. Rev. C **63**, 031301(R) (2001).
- [17] D. H. Youngblood, Y.-W. Lui, and H. L. Clark, Phys. Rev. C **65**, 034302 (2002).
- [18] B. John, Y. Tokimoto, Y.-W. Lui, H. Clark, and D. Youngblood, Phys. Rev. C **68**, 014305 (2003).
- [19] D. H. Youngblood *et al.*, Phys. Rev. C **69**, 034315 (2004).
- [20] D. H. Youngblood *et al.*, Phys. Rev. C **69**, 054312 (2004).
- [21] Y.-W. Lui *et al.*, Phys. Rev. C **70**, 014307 (2004).
- [22] Y.-W. Lui *et al.*, Phys. Rev. C **73**, 014314 (2006).
- [23] Y. Tokimoto *et al.*, Phys. Rev. C **74**, 044308 (2006).
- [24] D. H. Youngblood, Y.-W. Lui, and H. L. Clark, Phys. Rev. C **76**, 027304 (2007).

- [25] B. Bonin *et al.*, Nucl. Phys. A **430**, 349 (1984).
- [26] M. Hedden *et al.*, AIP Conf. Proc. **610**, 880 (2002).
- [27] M. Itoh *et al.*, Phys. Lett. B **549**, 58 (2002).
- [28] M. Uchida *et al.*, Phys. Lett. B **557**, 12 (2003).
- [29] M. Itoh *et al.*, Phys. Rev. C **68**, 064602 (2003).
- [30] M. Uchida *et al.*, Phys. Rev. C **69**, 051301(R) (2004).
- [31] U. Garg, Nucl. Phys. A **731**, 3 (2004).
- [32] M. Itoh *et al.*, Nucl. Phys. A **731**, 41 (2004).
- [33] B. K. Nayak *et al.*, Phys. Lett. B **637**, 43 (2006).
- [34] T. Li *et al.*, Phys. Rev. Lett. **99**, 162503 (2007).
- [35] U. Garg *et al.*, Nucl. Phys. A **788**, 36 (2007).
- [36] M. Fujiwara *et al.*, Nucl. Instrum. Meth. Phys. Res. A **422**, 484 (1999).
- [37] Y.-W. Lui, P. Bogucki, J. D. Bronson, D. H. Youngblood, and U. Garg, Phys. Rev. C **30**, 51 (1984).
- [38] James M. Lattimer and Madappa Prakash, Phys. Rep. **333**, 121 (2000).
- [39] J. M. Lattimer and M. Prakash, Science **304**, 532 (2004).
- [40] A. W. Steiner *et al.*, Phys. Rep. **411** (2005).
- [41] B.-A. Li and A. W. Steiner, Phys. Lett. B **642**, 436 (2006).
- [42] M. Itoh, Ph.D. thesis, Kyoto University (2003).
- [43] M. Itoh *et al.*, RCNP Annual Report p. 7 (1999).
- [44] S. Brandenburg *et al.*, Nuc. Phys. A **466**, 29 (1987).
- [45] G. R. Satchler and D. T. Khoa, Phys. Rev. C **55**, 285 (1997).
- [46] M. Rhoades-Brown, M. H. Macfarlane, and S. C. Pieper, Phys. Rev. C **21**, 2417 (1980).
- [47] M. Rhoades-Brown, M. H. Macfarlane, and S. C. Pieper, Phys. Rev. C **21**, 2436 (1980).
- [48] G. R. Satchler, Nucl. Phys. A **540** (1992).
- [49] L. D. Rickersten, unpublished (1976).
- [50] G. R. Satchler, Nucl. Phys. A **472** (1987).
- [51] M. N. Harakeh and A. E. L. Dieperink, Phys. Rev. C **23**, 2329 (1981).
- [52] G. Frickie *et al.*, At. Data Nucl. Data Tables **60**, 2 (1995).
- [53] S. Raman *et al.*, At. Data Nucl. Data Table **36** (1987).
- [54] R. H. Spear, At. Data Nucl. Data Table **42** (1989).

- [55] S. S. Dietrich and B. L. Berman, *At. Data Nucl. Data Tables* **38** (1988).
- [56] M. Hunyadi *et al.*, *Phys. Lett. B* **576**, 253 (2003).
- [57] B. K. Nayak *et al.*, *Phys. Lett. B* **674**, 281 (2009).
- [58] M. Hunyadi *et al.*, *Phys. Rev. C* **80**, 044317 (2009).
- [59] G. Colò *et al.*, *Phys. Lett. B* **485**, 362 (2000).
- [60] D. Vretenar, A. Wandelt, and P. Ring, *Phys. Lett. B* **485**, 334 (2000).
- [61] E. B. Balbutsev, I. V. Molodtsova, and A. V. Unzhakova, *Europhys. Lett.* **26**, 499 (1994).
- [62] V. Nesterenko, private communication.
- [63] J. M. Moss *et al.*, *Phys. Rev. Lett.* **37**, 816 (1976).
- [64] J. M. Moss *et al.*, *Phys. Rev. C* **18**, 741 (1978).
- [65] G. Colò *et al.*, *Phys. Rev. C* **70**, 024307 (2004).
- [66] G. Colò, private communication.
- [67] J. Piekarewicz, *Phys. Rev. C* **76**, 031301 (2007).
- [68] D. Vretenar, private communication.
- [69] V. Tselyaev *et al.*, *Phys. Rev. C* **79**, 034309 (2009).
- [70] S. Stringari, *Phys. Lett. B* **108**, 232 (1982).
- [71] O. Civitarese *et al.*, *Phys. Rev. C* **43**, 2622 (1991).
- [72] J. Piekarewicz and M. Centelles, *Phys. Rev. C* **79**, 054311 (2009).
- [73] B. G. Todd-Rutel and J. Piekarewicz, *Phys. Rev. Lett.* **95**, 122501 (2005).
- [74] G. A. Lalazissis *et al.*, *Phys. Rev. C* **55**, 540 (1997).
- [75] G. A. Lalazissis *et al.*, *Phys. Rev. C* **71**, 024312 (2003).
- [76] J. Piekarewicz, private communication.
- [77] J. Li *et al.*, *Phys. Rev. C* **78**, 064304 (2008).
- [78] J. Bartel *et al.*, *Nucl. Phys. A* **386**, 79 (1982).
- [79] E. Khan, *Phys. Rev. C* **80**, 011307 (2009).
- [80] E. Khan, *Phys. Rev. C* **80**, 057302 (2009).
- [81] D. Lunney *et al.*, *Rev. Mod. Phys.* **75**, 1021 (2003).
- [82] N. Zeldes *et al.*, *Nucl. Phys. A* **399**, 11 (1983).
- [83] M. N. Harakeh *et al.*, *Nucl. Phys. A* **327**, 373 (1979).
- [84] S. Patra *et al.*, *Phys. Rev. C* **65**, 044304 (2002).
- [85] S. Shlomo and D. H. Youngblood, *Phys. Rev. C* **47**, 529 (1993).

- [86] J. M. Pearson, Phys. Lett. B **271**, 12 (1991).
- [87] L.-W. Chen *et al.*, Phys. Rev. C **80**, 014322 (2009).
- [88] B.-A. Li and L.-W. Chen, Phys. Rev. C **72**, 064611 (2005).
- [89] Lie-Wen Chen, Che Ming Ko, and Bao-An Li, Phys. Rev. Lett **94**, 032701 (2005).
- [90] S. Yoshida and H. Sagawa, Phys. Rev. C **73**, 044320 (2006).
- [91] M. Centelles *et al.*, Phys. Rev. Lett. **102**, 122502 (2009).
- [92] H. Sagawa *et al.*, Phys. Rev. C **76**, 034327 (2007).
- [93] H. Baba *et al.*, Nucl. Phys. A **788**, 188c (2007).
- [94] C. Monrozeau *et al.*, Phys. Rev. Lett. **100**, 042501 (2008).
- [95] [http://www.gsi.de/fair/index\\_e.html](http://www.gsi.de/fair/index_e.html).
- [96] <http://www.frib.msu.edu/>.
- [97] B. K. Agrawal, S. Shlomo, and V. Kim Au, Phys. Rev. C **68**, 031304 (2003).
- [98] U. Garg, AIP Conf. Proc. **1128**, 100 (2009).
- [99] Lie-Wen Chen, Che Ming Ko, and Bao-An Li, Phys. Rev. C **72**, 064309 (2005).
- [100] D. N. Basu *et al.*, Phys. Rev. C **80**, 057304 (2009).